PHYSICAL REVIEW A **93**, 011601(R) (2016)

Mott transition for strongly interacting one-dimensional bosons in a shallow periodic potential

G. Boéris,[1] L. Gori,[2] M. D. Hoogerland,[3] A. Kumar,[2] E. Lucioni,[2] L. Tanzi,[2] M. Inguscio,[2,4] T. Giamarchi,[5] C. D'Errico,[2] G. Carleo,[1,*] G. Modugno,[2] and L. Sanchez-Palencia[1]

[1]*Laboratoire Charles Fabry, Institut d'Optique, CNRS, Univ Paris-Saclay, 2 avenue Augustin Fresnel, F-91127 Palaiseau cedex, France*

[2]*LENS and Dipartimento di Fisica e Astronomia, Università di Firenze, and CNR-INO 50019 Sesto Fiorentino, Italy*

[3]*Department of Physics, University of Auckland Private Bag 92019, Auckland, New Zealand*

[4]*INRIM, 10135 Torino, Italy*

[5]*Department of Quantum Matter Physics, University of Geneva, 24 quai Ernest-Ansermet, 1211 Geneva, Switzerland*

(Received 15 September 2015; published 4 January 2016)

We investigate the superfluid-insulator transition of one-dimensional interacting bosons in both deep and shallow periodic potentials. We compare a theoretical analysis based on quantum Monte Carlo simulations in continuum space and Luttinger liquid approach with experiments on ultracold atoms with tunable interactions and optical lattice depth. Experiments and theory are in excellent agreement. Our study provides a quantitative determination of the critical parameters for the Mott transition and defines the regimes of validity of widely used approximate models, namely, the Bose-Hubbard and sine-Gordon models.

DOI: 10.1103/PhysRevA.93.011601

Introduction. The interplay of repulsive interactions and a periodic potential in a quantum fluid triggers a superfluid-insulator transition known as the Mott transition, provided the potential period is commensurate to the inverse fluid density. The most familiar notion of Mott transition takes place in the limit of a deep periodic potential. In this case the lattice Hubbard model microscopically captures the dominant interaction and hopping processes, the strengths of which, U and J, strongly depend on the periodic potential amplitude V. Then, the Mott transition is driven by the competition of these sole two parameters at $J \sim U$ [1,2]. Quite strikingly in one dimension (1D) a Mott transition can exist even for a vanishingly small periodic potential provided the repulsive interactions are strong enough [3–6]. In the limit of a shallow potential, its amplitude V becomes subrelevant and the transition is mostly controlled by the interaction strength g alone [6].

Ultracold atoms provide a remarkable laboratory to study this physics [7,8]. So far the Mott transition has been observed in both deep [9–13] and shallow [14] optical lattices. Yet, the characterization of the Mott transition in shallow potentials remains a formidable challenge for both theory and experiments, with direct consequences not only in the ultracold atom realm but also in condensed matter for problems such as spin chains for instance [6,15,16].

On the theoretical side, while the Hubbard limit is now well documented [7,8,17] and its Mott transition has been extensively studied [18–25], its regime of validity beyond the deep-lattice limit is still largely unknown in 1D. Full *ab initio* results have been reported so far only for three dimensions (3D) [26], whereas a complete analysis of the 1D case is still in order, despite some recent progress [27–29]. In the limit of a vanishing potential, an estimate of the transition point may be nonetheless found in the sine-Gordon model whose coefficients are determined perturbatively [14,30]. This, however, ignores the unavoidable renormalization of the field-theoretic coupling parameters by the potential, which may significantly affect the transition. On the experimental side, the Mott transition has been clearly observed in the shallow lattice limit using modulation spectroscopy and transport measurements [14]. However, the experimental uncertainties did not allow for a precise determination of the phase diagram.

In this Rapid Communication, we report a quantitative joint theoretical and experimental investigation of the Mott transition for strongly interacting 1D bosons in a shallow periodic potential. Using continuous-space quantum Monte Carlo calculations, we determine the exact quantum phase diagram. Our calculations confirm the field-theoretical universal predictions and provide, in addition, accurate quantitative values of the critical parameters of the Mott transition. Experimentally, we perform transport measurements on a Bose gas with tunable interactions down to the limit of very shallow lattices and we analyze them with a phase slip based model to accurately determine the Mott transition. The numerical and experimental results are in excellent agreement and show significant deviation from the perturbative sine-Gordon theory using the *bare* Luttinger parameters.

Model and theoretical approach. We consider zero-temperature interacting 1D bosons of mass m with a contact interaction of strength g, subjected to a periodic potential $V(x) = V \sin^2(kx)$ of spacing $a = \pi/k$ and amplitude V. Both the large V and small V limits have the possibility of a Mott transition when the interactions are increased [17]. In spite of their qualitative different natures the two limiting cases are, however, expected to belong to the same universality class for they both lead to the same low-energy sine-Gordon model [4,6,17,31]. Within the Tomonaga-Luttinger liquid (TLL) approach, the homogeneous superfluid is parametrized by the Luttinger parameter K, which characterizes the interaction strength. For weak interactions, the periodic potential is essentially irrelevant, except in renormalizing the effective value of the Luttinger parameter. For strong interactions, the TLL may be unstable upon introducing a periodic potential, which then signals the Mott insulator phase. More precisely, two Mott transitions of different kinds should be distinguished.

*Present address: Theoretical Physics, ETH Zurich, 8093 Zurich, Switzerland.

The first one is triggered by changing the fluid density to commensurability at sufficiently strong interactions (Mott-δ transition), while the second one is triggered by increasing the interactions at commensurability (Mott-U transition). The TLL theory predicts the universal critical values $K_c = 1/p^2$ and $K_c = 2/p^2$ for the Mott-δ and Mott-U transitions, respectively, where p is the commensurability order [32–34].

Nevertheless, the TLL theory involves effective parameters that are not easily related to the microscopic Hamiltonian parameters and the critical curve $g_c(V)$ is presently not quantitatively known. To precisely determine the Mott transitions, we use quantum Monte Carlo (QMC) simulations. This allows us (i) to determine quantitatively the phase diagram in terms of the microscopic parameters and (ii) to compute explicitly the Luttinger parameter K as a function of the microscopic ones and make the link with field theory. We use the same implementation of the continuous-space worm algorithm [35,36] in the grand-canonical ensemble as used in Ref. [37], which is numerically exact for all the physical quantities we study in the following [38].

Incommensurate transition. We start with the incommensurate (Mott-δ) transition, which may be triggered by changing the chemical potential μ. In order to accurately determine the critical point, several key quantities are examined. These include the particle density n, the compressibility $\kappa \equiv \partial n/\partial\mu$, and the hydrodynamic superfluid density n_s, which are computed independently in the QMC simulations [38]. We then deduce the superfluid fraction $f_s = n_s/n$ and the Luttinger parameter $K = \pi\sqrt{(\hbar^2/m)n_s\kappa}$.

The QMC results are shown versus the chemical potential in the inset of Fig. 1 for $V = 2E_r$ where $E_r = \hbar^2k^2/2m$ is the recoil energy, $g = 7\hbar^2/ma$, and various system sizes. The density increases monotonically with the chemical potential μ and exhibits a plateau at commensurability, $na = 1$, where the superfluid density drops to zero. At the edges of the plateau, the compressibility shows marked cusps. This is the signature of the Mott-δ transition. The critical chemical potentials $\mu_c^{\pm}$ corresponding to the two edges of the plateau are accurately determined from the crossing points of the compressibility for different system sizes. They can also be found from the drop of the superfluid fraction f_s, which yields similar values for $\mu_c^{\pm}$. At the Mott-δ transition, the Luttinger parameter is expected to exhibit the universal discontinuity from $K = 1$ to $K = 0$. Our data are perfectly compatible with this prediction.

Repeating the same calculations for various values of the interaction strength, we find the Mott lobe in the g-μ plane shown in the main panel of Fig. 1. The black points and joining lines are determined from the $K = 1$ criterion, while the colored points are extracted from the crossing point of the compressibility (red), the cusp of the compressibility (green), and the crossing point of the Luttinger parameter (blue). The different methods yield results in excellent agreement all along the lobe within a few percent.

Commensurate transition. We now turn to the commensurate (Mott-U) transition. We vary the interaction strength $\gamma \equiv mg/\hbar^2n$ at commensurability ($na = 1$) and compute the one-body correlation function $g_1(x) = \langle\hat{\psi}^\dagger(x)\hat{\psi}(0)\rangle$, where $\hat{\psi}$ is the field operator [38]. When increasing γ along the line with $na = 1$ (red dashed line in Fig. 1), we observe a clear change of behavior of the g_1 function from algebraic for

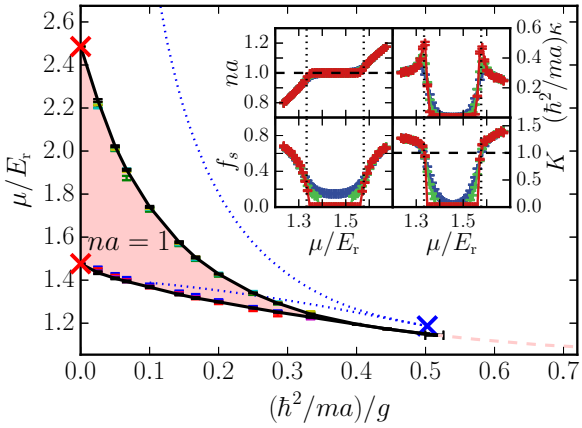

FIG. 1. QMC results for the phase diagram in the g-μ plane for a fixed amplitude of the periodic potential $V = 2E_r$. The black (dark) points joined by lines are determined from the $K = 1$ criterion. The crossing points of the compressibility (red), the position of the compressibility cusps (green), and the crossing points of the Luttinger parameter (blue) are also shown and are practically indiscernible. The left-hand red crosses are the hard-core limits [$(\hbar^2/ma)/g \to 0$]. The inside of the lobe (red shaded region) and the red dashed line correspond to a density of one particle per potential spacing. The blue dotted line is the prediction of the BH model and the right-hand blue cross is the corresponding tip of the lobe. Inset: The particle filling, na, the compressibility κ, the superfluid fraction f_s, and the Luttinger parameter K are shown versus the chemical potential μ, for a periodic potential amplitude $V = 2E_r$ and an interaction strength $g = 7\hbar^2/ma$. The various curves are the QMC results for different system sizes, $L/a = 30$, 50, and 100 (blue, green, and red, respectively), showing a sharper transition as the size increases. The vertical dotted lines show the transition points determined from the criterion $K = 1$.

$\gamma < \gamma_c$ to exponential for $\gamma > \gamma_c$ (see insets of Fig. 2). This is the signature of the Mott-U transition. The finite correlation length l_c in the insulating phase is shown in the left panel of Fig. 2. It is of only a few lattice sites long for strong interactions and increases up to a value comparable to the system size for $\gamma_c \sim 2$. This is compatible with the expected divergence of the correlation length at the transition. In the superfluid phase, the algebraic decay of the correlation function is compatible with the TLL theory prediction $g_1(x) \propto 1/x^{1/2K}$. The two values of the Luttinger parameter found from a fit to this prediction and from the thermodynamic prediction $K = \pi\sqrt{n_s\kappa}$ are in good agreement (see right panel of Fig. 2). When increasing the interaction towards the insulating phase, the Luttinger parameter decreases down to $K \simeq 2$ as predicted by the TLL theory.

To locate the Mott-U transition point accurately, we resort to the Berezinskii-Kosterlitz-Thouless renormalization group equations to perform the finite size scaling of the Luttinger parameter [38]. The results are shown in Fig. 3 (black points). In the strong potential limit, the results are compatible with the prediction of the Bose-Hubbard (BH) model with the critical value $(J/U)_c = 0.297 \pm 0.01$ [21,22] and the hopping J and interaction strength U calculated from the exact Wannier functions [20]. In the vanishing potential limit, the results converge to the critical value $\gamma_c(V = 0) \simeq 3.5$ (red cross in Fig. 3) found from the exact relation $K(\gamma)$ for the integrable

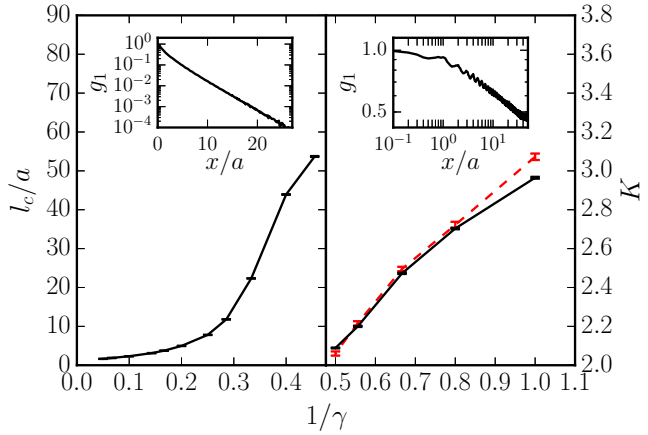

FIG. 2. Analysis of the correlation function $g_1(x) = \langle\hat{\psi}^\dagger(x)\hat{\psi}(0)\rangle$ for $V/E_r = 2$. The decay is exponential in the insulator (left inset, $\gamma = 7$) and algebraic in the superfluid (right inset, $\gamma = 1.25$). Left: Correlation length in the insulator. Right: Luttinger parameter in the superfluid extracted from the decay of the correlation function (solid black) and from the formula $K = \pi\sqrt{n_s\kappa}$ (dashed red). The QMC results are the points, connected by straight lines to guide the eye. Note that the inflection of the correlation length curve close to the transition is due to finite size effects.

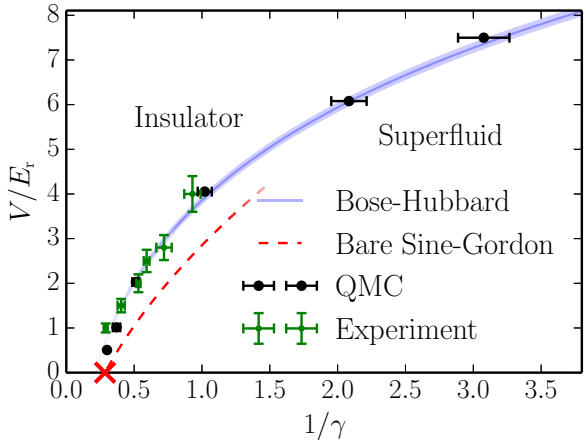

FIG. 3. Phase diagram in the g-V plane at commensurability ($na = 1$). The big black and small green points (both with error bars) are the Monte Carlo and experimental results, respectively. The solid blue line is the BH prediction using exact Wannier functions and the critical value $(J/U)_c = 0.297 \pm 0.01$ (the shaded area corresponds to this error bar). The red cross indicates the critical interaction strength g_c such that $K(g_c) = 2$ in the Lieb-Liniger model. Along the whole transition line the *effective* Luttinger parameter remains $K = 2$. The dashed red line is the result of the *bare* sine-Gordon theory [30].

Lieb-Liniger model [39]. However, in the intermediate regime, we find a strong deviation from the pinning transition line (red dashed line) computed in Ref. [30] from the perturbative sine-Gordon theory using the *bare* Luttinger parameters. This shows that to quantitatively obtain the phase diagram the renormalization of the Luttinger parameters even by relatively weak interactions is significant and cannot be ignored in the perturbative field theory.

Experiment. The experiment starts with a Bose-Einstein condensate of ^{39}K with tunable scattering length at a broad Feshbach resonance [40]. The condensate is split into about 1000 vertical 1D tubes by adiabatically raising a strong 2D horizontal optical lattice. Each tube contains on average 36 atoms and the transverse trapping frequency, $\omega_\perp = 2\pi\times 40$ kHz corresponds to an energy higher than all other energy scales, realizing an effective 1D geometry. In the longitudinal direction we then adiabatically raise a weak optical lattice with spacing $a = \lambda/2 = 532$ nm and normalized amplitude V/E_r ranging from 1.0(1) to 4.0(4). A magnetic field holds the system against gravity and a longitudinal harmonic trap potential, with frequency $\omega_z = 2\pi\times 160$ Hz, makes it inhomogeneous. By varying the 3D scattering length a_{3D}, we can tune the Lieb-Liniger parameter γ in the range 0.07–7.4. The system parameters are chosen to obtain a mean filling $\langle na\rangle = 1$. This implies that in most of the tubes there are one or two regions with local commensurate filling, $na = 1$, which can undergo a Mott-U transition. There is, however, a fraction of tubes with $na < 1$ that cannot become insulating [38].

To detect the Mott transition we excite a sloshing motion of the system through a shift of the trapping potential, obtained by suddenly switching off the magnetic field gradient [14,41]. We let the atoms evolve in the trap for a variable time t, after which all optical potentials are switched off and time-of-flight absorption images are recorded. An example of the time evolution of the momentum distribution peak $p(t)$ is shown in the inset of Fig. 4: an initial increase of $p(t)$ up to a certain critical value p_c is followed by a subsequent decrease. We analyze this behavior in the frame of a phase slip based model [41–43]. Phase slips, i.e., the dominant excitations in 1D, make the system dynamics dissipative: at short times where $p(t) < p_c$, the data can be fit with a damped oscillation function $p(t) = p_{\max}e^{-Gt}\sin(\omega' t)$, where ω' is the renormalized frequency taking into account the damping rate G and the presence of the lattice; at larger times the system enters a dynamically unstable (insulating) regime driven by a divergence of the phase slip rate [41]. The critical momentum p_c for the occurrence of the dynamical instability, is identified as the momentum value where the experimental data points deviate with respect to the theoretical curve [38].

The critical momentum is expected to vanish at the superfluid-insulator transition [42]. The behavior of p_c as a function of the scattering length a_{3D} is reported in Fig. 4 for several values of the lattice depth. The measured p_c initially decreases for increasing a_{3D} and then reaches a finite constant value. We interpret the onset of the plateau as the critical scattering length a_c to enter the Mott regime for the commensurate regions of the system: transport along the corresponding tubes is globally suppressed driving the system into an effective insulating regime. The fraction of tubes that does not reach the critical density $na = 1$ keeps instead moving also for $a_{3D} > a_c$, originating the observed plateau for p_c. For each set of measurements with a given value of V, we determine a_c by means of a piecewise fit. We use a second-order polynomial fit, which is justified by the phase slip based model [38,42,44]. We clearly see that as V decreases, a_c—and thus also γ_c—increases.

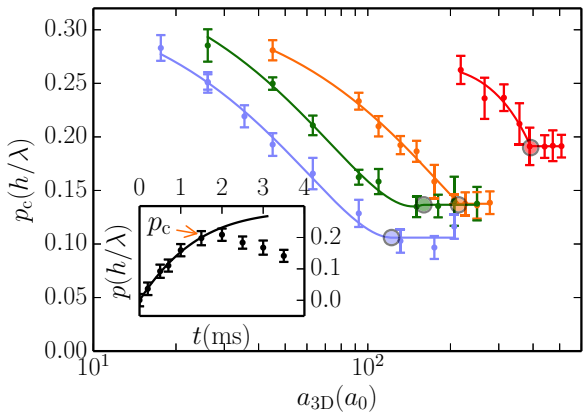

FIG. 4. Critical momentum p_c versus scattering length a_{3D} for four lattice depths: From right to left, $V/E_r = 1$ (red), 2 (orange), 2.8 (green), 4 (blue). A piecewise fit (solid lines) determines the critical values for the superfluid–Mott insulator transition (circles): respectively, $a_c/a_0 = 392 \pm 12, 214 \pm 6, 160 \pm 30, 122 \pm 8$. The error bars derive from the procedure to obtain p_c [38]. Inset: time evolution of the momentum distribution peak p for $a_{3D} = 109a_0$ and $V/E_r = 2$. The solid line is the theoretical damped oscillation fitting the data for $p < p_c$ before the dynamical instability sets in. The error bars comprise the imaging resolution and the statistical uncertainties.

For each value of lattice depth we get the Mott-U transition point converting a_c into γ_c for $na = 1$. The experimental results are shown as green points in Fig. 3. Within our uncertainties [45], the experiment is in very good agreement with the numerical simulations. Our results are also consistent with those reported in Ref. [14] within the uncertainties. Our experiment confirms the clear deviation of the transition line from the bare sine-Gordon prediction found by the QMC calculations. Note that, surprisingly enough, while the BH model is justified only for $V \gg E_r$, both numerics and experiment show that the BH prediction for the Mott-U transition is quite accurate down to the limit $V \to 0$. This agreement is, however, rather accidental and the breakdown of the BH model is manifest in other quantities. For instance, the BH prediction for the Mott lobe deviates significantly from the exact QMC result (see Fig. 1). In particular, the Mott gap $\Delta = \mu_c^+ - \mu_c^-$ is largely overestimated by the BH prediction.

Conclusions. We have studied, both theoretically and experimentally, the Mott transition of strongly interacting 1D bosons in a periodic potential from deep to shallow potentials. Our *ab initio* QMC calculations validate the field-theoretic universal predictions and, in addition, provide a quantitative determination of the phase diagram. Our results show that the renormalization of the Luttinger parameter is significant even for weak periodic potentials. The numerical analysis gives excellent agreement with experiments for the Mott-U transition. The experimental observation of our numerical phase diagram for the Mott-δ transition is still beyond reach for ultracold atomic systems due to the requirement of a fine control of atom number in box-shaped potentials. In spite of recent progress in that direction [46–48], it remains a great challenge for future studies.

Note added. Recently, a preprint appeared reporting the numerical study of the Mott-U transition with results consistent with ours [49].

Acknowledgments. This research was supported by the European Union FET-Proactive QUIC (H2020 Grant No. 641122), the European Research Council ERC-StG ALoGlaDis (FP7/2007-2013 Grant No. 256294), the European Union Marie Curie IEF (FP7/2007-2013 Grant No. 327143), the French Ministère de l'Enseignement Supérieur et de la Recherche, the Italian Ministero dell'Istruzione, dell'Universita e della Ricerca (Grant No. RBFR12NLNA), and the Swiss NSF under Division II. Numerical calculations were performed using High Performance Cluster resources from GENCI-CCRT/CINES (Grant No. c2015056853) and the computing facility cluster Grappe Massivement Parallèle de Calcul Scientifique (GMPCS) of the Fédération de Recherche Lumière-Matière (FR LUMAT 2764), and make use of the ALPS scheduler library and statistical analysis tools [50–52].

[1] N. Mott, Proc. R. Soc. London, Ser. A **62**, 416 (1949).
[2] N. F. Mott, *Metal-Insulator Transitions* (Taylor & Francis, London, UK, 1990).
[3] F. D. M. Haldane, J. Phys. Lett. A **80**, 281 (1980).
[4] F. D. M. Haldane, Phys. Rev. Lett. **47**, 1840 (1981).
[5] T. Giamarchi, Physica B **230–232**, 975 (1997).
[6] T. Giamarchi, *Quantum Physics in One Dimension* (Carendon, Oxford, 2004).
[7] M. Lewenstein, A. Sanpera, V. Ahufinger, B. Damski, A. Sen, and U. Sen, Adv. Phys. **56**, 243 (2007).
[8] I. Bloch, J. Dalibard, and W. Zwerger, Rev. Mod. Phys. **80**, 885 (2008).
[9] M. Greiner, O. Mandel, T. Esslinger, T. W. Hänsch, and I. Bloch, Nature (London) **415**, 39 (2002).
[10] T. Stöferle, H. Moritz, C. Schori, M. Köhl, and T. Esslinger, Phys. Rev. Lett. **92**, 130403 (2003).
[11] M. Köhl, H. Moritz, T. Stöferle, C. Schori, and T. Esslinger, J. Low Temp. Phys. **138**, 635 (2005).
[12] R. Jördens, N. Strohmaier, K. Günter, H. Moritz, and T. Esslinger, Nature (London) **455**, 204 (2008).
[13] U. Schneider, L. Hackermüller, S. Will, T. Best, I. Bloch, T. A. Costi, R. W. Helmes, D. Rasch, and A. Rosch, Science **322**, 1520 (2008).
[14] E. Haller, R. Hart, M. J. Mark, J. G. Danzl, L. Reichsöllner, M. Gustavsson, M. Dalmonte, G. Pupillo, and H.-C. Nägerl, Nature (London) **466**, 597 (2010).
[15] M. Oshikawa and I. Affleck, Phys. Rev. Lett. **79**, 2883 (1997).
[16] J.-P. Pouget, Eur. Phys. J. B **20**, 321 (2001); **24**, 415(E) (2001).
[17] A. Georges and T. Giamarchi, in *Many-Body Physics with Ultracold Gases*, edited by Christophe Salomon, Georgy V. Shlyapnikov, and Leticia F. Cugliandolo, Proceedings of the Les Houches Summer School of Theoretical Physics Vol. XCIV

(Oxford University Press, Oxford, 2012), Chap., Strongly correlated bosons and fermions in optical lattices.
[18] M. P. A. Fisher, P. B. Weichman, G. Grinstein, and D. S. Fisher, Phys. Rev. B **40**, 546 (1989).
[19] G. G. Batrouni, R. T. Scalettar, and G. T. Zimanyi, Phys. Rev. Lett. **65**, 1765 (1990).
[20] D. Jaksch, C. Bruder, J. I. Cirac, C. W. Gardiner, and P. Zoller, Phys. Rev. Lett. **81**, 3108 (1998).
[21] T. D. Kühner and H. Monien, Phys. Rev. B **58**, R14741(R) (1998).
[22] T. D. Kühner, S. R. White, and H. Monien, Phys. Rev. B **61**, 12474 (2000).
[23] B. Capogrosso-Sansone, N. V. Prokof'ev, and B. V. Svistunov, Phys. Rev. B **75**, 134302 (2007).
[24] M. J. Mark, E. Haller, K. Lauber, J. G. Danzl, A. J. Daley, and H.-C. Nägerl, Phys. Rev. Lett. **107**, 175301 (2011).
[25] J. Carrasquilla, S. R. Manmana, and M. Rigol, Phys. Rev. A **87**, 043606 (2013).
[26] S. Pilati and M. Troyer, Phys. Rev. Lett. **108**, 155301 (2012).
[27] F. De Soto and M. C. Gordillo, J. Low Temp. Phys. **171**, 348 (2012).
[28] C. Carbonell-Coronado, F. De Soto, and M. C. Gordillo, Phys. Rev. A **87**, 063631 (2013).
[29] T. Sowinski, J. Opt. Soc. Am. B **32**, 670 (2015).
[30] H.-P. Büchler, G. Blatter, and W. Zwerger, Phys. Rev. Lett. **90**, 130401 (2003).
[31] M. A. Cazalilla, R. Citro, T. Giamarchi, E. Orignac, and M. Rigol, Rev. Mod. Phys. **83**, 1405 (2011).
[32] H. J. Schulz, Phys. Rev. B **22**, 5274 (1980).
[33] T. Giamarchi, Phys. Rev. B **46**, 342 (1992).
[34] E. B. Kolomeisky, Phys. Rev. B **47**, 6193 (1993).
[35] M. Boninsegni, N. Prokof'ev, and B. Svistunov, Phys. Rev. Lett. **96**, 070601 (2006).
[36] M. Boninsegni, N. V. Prokof'ev, and B. V. Svistunov, Phys. Rev. E **74**, 036701 (2006).
[37] G. Carleo, G. Boéris, M. Holzmann, and L. Sanchez-Palencia, Phys. Rev. Lett. **111**, 050406 (2013).
[38] See Supplemental Material at http://link.aps.org/supplemental/10.1103/PhysRevA.93.011601 for (i) Quantum Monte Carlo calculations; (ii) Superfluid density; (iii) Finite size scaling; (iv) Experimental methods.
[39] E. H. Lieb and W. Liniger, Phys. Rev. **130**, 1605 (1963).
[40] G. Roati, M. Zaccanti, C. D'Errico, J. Catani, M. Modugno, A. Simoni, M. Inguscio, and G. Modugno, Phys. Rev. Lett. **99**, 010403 (2007).
[41] L. Tanzi, E. Lucioni, S. Chaudhuri, L. Gori, A. Kumar, C. D'Errico, M. Inguscio, and G. Modugno, Phys. Rev. Lett. **111**, 115301 (2013).
[42] A. Polkovnikov, E. Altman, E. Demler, B. Halperin, and M. D. Lukin, Phys. Rev. A **71**, 063613 (2005).
[43] D. McKay, M. White, M. Pasienski, and B. DeMarco, Nature (London) **453**, 76 (2008).
[44] I. Danshita and A. Polkovnikov, Phys. Rev. A **85**, 023638 (2012).
[45] The horizontal error bars derive from the fitted a_c while the vertical ones are due to the 10% of uncertainty in the Raman-Nath diffraction technique employed for the calibration of periodic potential amplitude.
[46] T. P. Meyrath, F. Schreck, J. L. Hanssen, C.-S. Chuu, and M. G. Raizen, Phys. Rev. A **71**, 041604 (2005).
[47] A. L. Gaunt, T. F. Schmidutz, I. Gotlibovych, R. P. Smith, and Z. Hadzibabic, Phys. Rev. Lett. **110**, 200406 (2013).
[48] L. Chomaz, L. Corman, T. Bienaimé, R. Desbuquois, C. Weitenberg, S. Nascimbène, J. Beugnon, and J. Dalibard, Nat. Commun. **6**, 6162 (2015).
[49] G. E. Astrakharchik, K. V. Krutitsky, M. Lewenstein, and F. Mazzanti, arXiv:1509.01424.
[50] M. Troyer, B. Ammon, and E. Heeb, Lect. Notes Comput. Sci. **1505**, 191 (1998).
[51] A. Albuquerque, F. Alet, P. Corboz, P. Dayal, A. Feiguin, S. Fuchs, L. Gamper, E. Gull, S. Guertler, A. Honecker *et al.*, J. Magn. Magn. Mater. **310**, 1187 (2007).
[52] B. Bauer, L. D. Carr, H. Evertz, A. Feiguin, J. Freire, S. Fuchs, L. Gamper, J. Gukelberger, E. Gull, S. Guertler *et al.*, J. Stat. Mech.: Theor. Exp. (2011) P05001.

–*Supplemental Material*–
Mott transition for strongly-interacting 1D Bosons in a shallow periodic potential

G. Boéris,[1] L. Gori,[2] M. D. Hoogerland,[3] A. Kumar,[2] E. Lucioni,[2] L. Tanzi,[2] M. Inguscio,[2,4]
T. Giamarchi,[5] C. D'Errico,[2] G. Carleo,[1,*] G. Modugno,[2] and L. Sanchez-Palencia[1]

[1]*Laboratoire Charles Fabry, Institut d'Optique, CNRS, Univ Paris-Saclay, 2 avenue Augustin Fresnel, F-91127 Palaiseau cedex, France*
[2]*LENS and Dipartimento di Fisica e Astronomia, Università di Firenze, and CNR-INO 50019 Sesto Fiorentino Italy*
[3]*Department of Physics, University of Auckland Private Bag 92019, Auckland, New Zealand*
[4]*INRIM, 10135 Torino, Italy*
[5]*Department of Quantum Matter Physics, University of Geneva, 24 quai Ernest-Ansermet, 1211 Geneva, Switzerland*

(Dated: December 14, 2015)

In this Supplemental Material we give additional details on the methods and the analysis we have performed in the main text of our Rapid Communication. In particular we provide a detailed description of i) the quantum Monte Carlo calculations, ii) the determination of the physical quantities, iii) the finite-size scaling analysis, and iv) the experimental methods.

Quantum Monte Carlo calculations

We consider 1D interacting bosons at zero temperature governed by the continuos-space Hamiltonian,

$$\hat{H} = \int \mathrm{d}x \left[\frac{\hbar^2}{2m} \nabla\hat{\psi}^\dagger \nabla\hat{\psi} + \frac{g}{2}\hat{\psi}^\dagger\hat{\psi}^\dagger\hat{\psi}\hat{\psi} + V(x)\hat{\psi}^\dagger\hat{\psi} \right], \quad (1)$$

where $\hat{\psi}(x)$ is the Bose field, m is the particle mass, g is the contact interaction strength, and $V(x) = V\sin^2(kx)$ is a periodic potential of spacing $a = \pi/k$ and amplitude V.

We study the interacting quantum system from first principles, by means of quantum Monte Carlo (QMC) numerical simulations. Path-integral QMC approaches allow us to compute the exact thermodynamic properties of a generic, interacting bosonic quantum system in any dimensions. This is achieved by means of the path-integral representation of the grand-canonical partition function $Z = \mathrm{Tr}[e^{-\beta(\hat{H}-\mu\hat{N})}]$, where $\beta = 1/k_{\mathrm{B}}T$ with k_{B} the Boltzmann constant and T the temperature, μ is the chemical potential, and $\hat{N} = \int \mathrm{d}x\, \hat{\psi}^\dagger\psi$ is the total particle number operator. The quantum partition function is expressed as an equivalent classical partition function of interacting polymers living in dimension $D+1$, where the additional dimension is the imaginary-time direction [1]. The equivalent classical partition function can be treated stochastically by means of Monte Carlo sampling. An efficient way of sampling the associated partition function is given by the worm algorithm [2, 3].

In our implementation, the imaginary-time propagator entering the path-integral representation is written as

$$\langle \{\mathbf{r}_i\}|e^{-\varepsilon\hat{H}}|\{\mathbf{r}'_i\}\rangle = \prod_{i=1}^{N} \rho_\varepsilon^{(0)}(\mathbf{r}_i,\mathbf{r}'_i) \prod_{i=1}^{N} e^{-U_\varepsilon^{(1)}(\mathbf{r}_i,\mathbf{r}'_i)} \times \times \prod_{i<j} e^{-U_\varepsilon^{(2)}(\mathbf{r}_i,\mathbf{r}_j,\mathbf{r}'_i,\mathbf{r}'_j)}, \quad (2)$$

where $\rho_\varepsilon^{(0)}(\mathbf{r}_i,\mathbf{r}'_i) = \sqrt{m/2\pi\hbar^2\varepsilon} \times e^{-m|\mathbf{r}_i-\mathbf{r}'_i|^2/2\hbar^2\varepsilon}$ is the free-particle propagator. The one-body contribution $e^{-U_\varepsilon^{(1)}(\mathbf{r}_i,\mathbf{r}'_i)} = \langle \mathbf{r}_i|e^{-\varepsilon[\hat{\mathbf{p}}^2/2m+V(\hat{\mathbf{r}})]}|\mathbf{r}'_i\rangle / \rho_\varepsilon^{(0)}(\mathbf{r}_i,\mathbf{r}'_i)$ is computed exactly by matrix squaring [1]. The two-body interaction is taken into account at the pair-product level, thanks to the explicit expression for the two-body propagator $e^{-U_\varepsilon^{(2)}(\mathbf{r}_i,\mathbf{r}_j,\mathbf{r}'_i,\mathbf{r}'_j)} = \langle \mathbf{r}_i,\mathbf{r}_j|e^{-\varepsilon[(\hat{\mathbf{p}}_i^2+\hat{\mathbf{p}}_j^2)/2m)+g\delta(\hat{\mathbf{r}}_i-\hat{\mathbf{r}}_j)]}|\mathbf{r}'_i,\mathbf{r}'_j\rangle / \rho_\varepsilon^{(0)}(\mathbf{r}_i,\mathbf{r}'_i)\rho_\varepsilon^{(0)}(\mathbf{r}_j,\mathbf{r}'_j)$, which is known [4]. The systematic error coming from the discretization of the path-integral along the imaginary-time direction is smaller than the statistical errorbars reported in our results.

Determination of physical quantities in QMC calculations

In the Rapid Communication, several quantities are examined to accurately determine the Mott transition critical point. The particle density $n = \int \mathrm{d}x \langle \psi^\dagger(x)\psi(x)\rangle / L$ is computed directly in the path integral formulation. The compressibility $\kappa = \partial n/\partial\mu$ is calculated independently from the particle number fluctuations, using the relation $\kappa = \frac{\beta}{L}\langle (N-\langle N\rangle)^2\rangle$ so as to significantly suppress statistical fluctuations.

The stiffness $\Upsilon_{\mathrm{s}} = -\frac{mL}{\beta\hbar^2}\frac{\partial^2 \ln Z}{\partial\theta_0^2}\Big|_0$ measures the response of the system when the periodic boundary conditions are twisted by an angle θ_0. It is directly computed by QMC using the usual winding number estimator [1]. However, this quantity strongly depends on the ratio β/L [5]. The relevant quantity to study is the superfluid density n_{s} appearing in the hydrodynamic action

$$S[\theta] = \int_0^L \mathrm{d}x \int_0^{\hbar\beta} \mathrm{d}\tau \left[\frac{\hbar^2 n_{\mathrm{s}}}{2m}(\partial_x\theta)^2 + \frac{\hbar^2\kappa}{2}(\partial_\tau\theta)^2 \right]. \quad (3)$$

Computing the partition function $Z = \int \mathscr{D}\theta\, e^{-S[\theta]/\hbar}$, correctly taking into account winding configurations of the form $\theta(x,\tau) = 2\pi kx/L$ with $k \in \mathbb{Z}$, one deduces the relation

$$\Upsilon_{\mathrm{s}} = n_{\mathrm{s}} \left(1 - 4\pi^2 n_{\mathrm{s}} \frac{\hbar^2\beta}{mL} \frac{\sum_{k=-\infty}^{+\infty} k^2 e^{-2\pi^2 n_{\mathrm{s}} k^2\hbar^2\beta/mL}}{\sum_{k=-\infty}^{+\infty} e^{-2\pi^2 n_{\mathrm{s}} k^2\hbar^2\beta/mL}} \right). \quad (4)$$

In our calculations, we invert this relation and extract n_s from the stiffness Υ_s computed by QMC.

The one-body density-matrix $g_1(x) = \langle \hat{\psi}^\dagger(x)\hat{\psi}(0)\rangle$ can be also computed exactly by means of the worm algorithm. This algorithm efficiently samples an extended configuration space which contains both closed polymers (world lines) as well as configurations with two open ends (informally known as the *worm*). The former configurations correspond to the partition function Z, while the latter yield a contribution proportional to the one-body density matrix. It has been shown that sampling this enlarged space has the twofold advantage of both substantially alleviating the critical slowing down in Monte Carlo sampling, and yielding direct access to $g_1(x)$ [2, 3].

Finite-size scaling

To precisely determine the Mott-U critical interaction strength g_c, we study the evolution of the Luttinger parameter K for the increasing system sizes $L/a = 30$, 50, and 100. When L is increased, the temperature T is lowered by keeping the ratio β/L constant in order to consistently compute the ground-state properties. We resort to the known Berezinkii-Kosterlitz-Thouless (BKT) renormalization group (RG) equations to perform the finite-size scaling and determine the critical interaction strength in the thermodynamic limit. In particular, the finite-size behaviour of the Luttinger parameter K and of renormalized potential strength V are governed by the renormalization equations [6–10],

$$\frac{\mathrm{d}K}{\mathrm{d}\ell} = -\frac{\pi^6}{16}\left(\frac{V}{E_r}\right)^2 K^2 \quad ; \quad \frac{\mathrm{d}V}{\mathrm{d}\ell} = (2-K)V. \tag{5}$$

Dividing these two equations one by another, one finds that the quantity

$$\zeta \equiv \frac{2}{K} + \ln\left(\frac{K}{2}\right) - \frac{\pi^2}{16}\left(\frac{V}{E_r}\right)^2 \tag{6}$$

is conserved along the RG trajectories. The separatrix between the superfluid and the insulating phases then corresponds to $K = 2$ and $V = 0$, i.e. $\zeta = 1$. In practice, we use the values of the Luttinger parameter K_1 and K_2 for two system sizes L_1 and L_2, and compute ζ using the integral relation

$$\int_{K_2}^{K_1} \frac{\mathrm{d}K}{K^2(\ln K/2 - \zeta) + 2K} = \ln(L_2/L_1). \tag{7}$$

The Mott-U critical point is then determined using the criterion $\zeta = 1$.

Experimental methods

In the experiment, a Bose-Einstein condensate of ^{39}K atoms is split in about 10^3 1D subsystems (potential tubes) by means of a 2D optical lattice. The overall Thomas-Fermi distribution of atoms in the tube labelled by i and j along the two horizontal directions is given by $N_{i,j} = N_{0,0}[1 - 2\pi N_{0,0}(i^2 + j^2)/5N_T]^{3/2}$, where $N_T = 3.5 \times 10^4$ is the total atom number and $N_{0,0} \simeq 50$ is the atom number in the central tube. On N_T there is a 6% statistical error while a 30% systematic uncertainty is due to the imaging calibration. Along the vertical direction of the tube, where we load the weak periodic potential, the trapping frequency is $\omega_z = 2\pi \times 160$ Hz. A good estimate of the mean atomic density for each tube is provided by the largest of the Thomas-Fermi and the Tonks values [11]. The mean site occupation $\langle na\rangle$ is then calculated by averaging over all the tubes. During the lattice loading we employ an optimal value of the 3D scattering length to get commensurability on average, i.e. $\langle na\rangle = 1$. Given ω_z and N_T, the optimal value is $a_{3D} = 220\,a_0$. The temperature of the system, $T \simeq 30$ nK [12], is below the 1D degeneracy temperature $T_D \simeq 50$ nK [13].

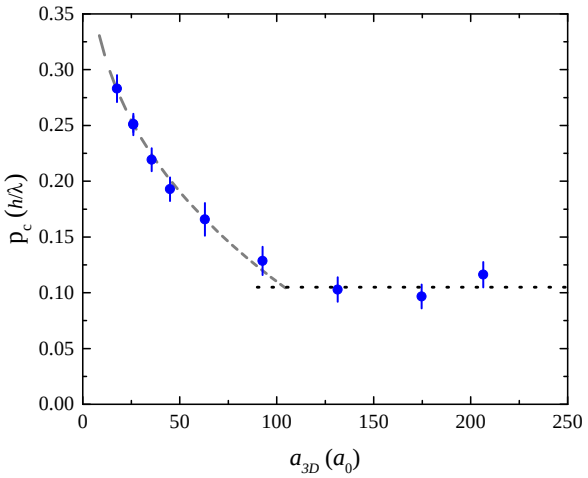

Figure 1. For $V/E_R = 4$ the experimental critical momentum (blue dots) is compared to the one predicted by the quantum phase slip based model, which applies up to the critical scattering length a_c to enter the MI regime (gray dashed line). For $a > a_c$, p_c has instead a plateau due to tubes with occupation $na < 1$ (black dotted line).

After the lattice loading, by varying the 3D scattering length a_{3D}, we tune the 1D scattering length $a_{1D} = \ell_\perp^2(1 - 1.03a_{3D}/\ell_\perp)/2a_{3D}$, and thus the Lieb-Liniger parameter γ, where $\ell_\perp = \sqrt{\hbar/m\omega_\perp}$ is the harmonic transverse size of a tube, fixed by the 2D lattice. The value of γ is estimated by averaging over all the tubes $1/(n_{max}aa_{1D})$, where the peak occupation $n_{max}a$ is the largest of the Thomas-Fermi and the Tonks values. The mean peak occupation, i.e. the peak occupation averaged over all the tubes, is $\langle n_{max}a\rangle \simeq 1.2$ and the peak density in the central tube is less than two, thus preventing localization mechanisms at occupations other than one. Despite the inhomogeneity of our system, at sufficiently strong interactions we clearly observe a suppression of the system dynamics. We interpret the latter as due to the fact that within each tube, a part of the atoms reaches the localization condition $na = 1$ stopping also the remaining adjacent parts with different occupation. We estimate that about one quarter of the atoms resides in tubes where the occupation is always $na < 1$,

producing the plateau in p_c shown in Fig. 4 of the main paper. We note that for a given lattice depth, when increasing the scattering length in the Mott phase ($a_{3D} > a_c$), this fraction of delocalized atoms remains constant because in the tubes where the Mott domains form the density is fixed. This interpretation is corroborated by the observed increase of p_c at the plateau for decreasing V, since the increase of the interaction strength that is necessary to reach the insulating regime produces an overall decrease of the density of the 1D systems, hence an increase of the fraction of tubes that does not reach $na = 1$.

The complete model we use to fit the time dependence of the momentum, $p(t)$, as shown in the inset of Fig. 4 of the main paper, is $p(t) = p_{max} e^{-Gt} \sin(\omega' t)$ with amplitude $p_{max} = m^* \omega^{*2} z_0/\omega'$, frequency $\omega' = \sqrt{\omega^{*2} - G^2}$ and damping rate G. Here m^* is the effective mass due to the shallow lattice, $z_0 \simeq 3\,\mu$m is the trap displacement, and $\omega^* = \omega_z \sqrt{m/m^*}$ is the lattice renormalized frequency. As described in Ref. [14], the critical momentum p_c is determined in the following way. The difference between the theoretical curve describing the initial damped motion and the experimental data is plot as a function of time. The onset of the deviation of the experimental data points with respect to the theoretical curve, is then determined by fitting such a plot with a linear piece-wise function. From such a fit we finally obtain the correspondent momentum, p_c, and its uncertainty.

In the absence of an exact theoretical model for obtaining the critical momentum to enter the dynamical instability regime at finite interaction, we use a quantum phase slips based model to predict the interaction dependence of p_c. Along the lines of Ref. [14] we use the equation for the quantum phase slip nucleation rate [15, 16]

$$\begin{aligned}\Gamma =& B L(U) \sqrt{naJU}\, \sqrt{\pi/2 - p\lambda/2\hbar} \times \\ & \sqrt{\frac{7.1(\pi/2 - p\lambda/2\hbar)^{5/2}}{2\pi\sqrt{U/naJ}}} \times \\ & \exp\left[-7.1\sqrt{naJ/U}(\pi/2 - p\lambda/2\hbar)^{5/2}\right] . \end{aligned} \tag{8}$$

Here $L(U) \simeq 2U^{1/3}$ is the mean length of the tubes and B is a phenomenological constant. Assuming that the system enters the strongly dissipative regime when the nucleation rate Γ exceeds a constant critical value, from Eq. (8) we can obtain p_c for each given value of the interaction U. Since this relation is valid in the Bose-Hubbard regime, we can employ it to estimate the critical momentum $p_c(U)$ for the experimental case with $V/E_R = 4$. The phenomenological parameter B is arbitrarily adjusted to reproduce the measured p_c at one interaction value, $U = 2.4J$. In Fig. 1 we compare the measured and the predicted p_c as a function of the scattering length $a_{3D} \propto U$. The quantum phase slip-based model well reproduces the experimental behaviour of p_c with the interaction, showing a quadratic dependence of p_c on a_{3D}. This result justifies the choice of a quadratic polynomial fit in Fig. 4 of the main paper, at least for the measurements with larger V. For shallower lattices the Tomonaga-Luttinger Liquid model for the nucleation rate could in principle be used [15], but this would require the Luttinger parameter K as a function of the interaction γ in the presence of the lattice, which is still unknown.

* Current address: Theoretical Physics, ETH Zurich, 8093 Zurich, Switzerland

[1] D. M. Ceperley, Rev. Mod. Phys. **67**, 279 (1995).
[2] M. Boninsegni, N. Prokof'ev, and B. Svistunov, Phys. Rev. Lett. **96**, 070601 (2006).
[3] M. Boninsegni, N. V. Prokof'ev, and B. V. Svistunov, Phys. Rev. E **74**, 036701 (2006).
[4] B. Gaveau and L. S. Schulman, J. Phys. A **19**, 1833 (1986).
[5] N. V. Prokof'ev and B. V. Svistunov, Phys. Rev. B **61**, 11282 (2000).
[6] V. L. Berezinskii, Sov. Phys. JETP **34**, 610 (1972).
[7] J. M. Kosterlitz and D. J. Thouless, J. Phys. C: Solid State Phys. **6**, 1181 (1973).
[8] N. Prokof'ev, O. Ruebenacker, and B. Svistunov, Phys. Rev. Lett. **87**, 270402 (2001).
[9] N. Prokof'ev and B. Svistunov, Phys. Rev. A **66**, 043608 (2002).
[10] T. Giamarchi, *Quantum Physics in One Dimension* (Carendon press, Oxford, 2004).
[11] V. Dunjko, V. Lorent, and M. Olshanii, Phys. Rev. Lett. **86**, 5413 (2001).
[12] S. Richard, F. Gerbier, J. H. Thywissen, M. Hugbart, P. Bouyer, and A. Aspect, Phys. Rev. Lett. **91**, 010405 (2003).
[13] D. S. Petrov, G. V. Shlyapnikov, and J. T. M. Walraven, Phys. Rev. Lett. **85**, 3745 (2000).
[14] L. Tanzi, E. Lucioni, S. Chaudhuri, L. Gori, A. Kumar, C. D'Errico, M. Inguscio, and G. Modugno, Phys. Rev. Lett. **111**, 115301 (2013).
[15] A. Polkovnikov, E. Altman, E. Demler, B. Halperin, and M. D. Lukin, Phys. Rev. A **71**, 063613 (2005).
[16] I. Danshita and A. Polkovnikov, Phys. Rev. A **85**, 023638 (2012).